

Implicit Discriminative Knowledge Learning for Visible-Infrared Person Re-Identification

Kaijie Ren, Lei Zhang*

School of Microelectronics and Communication Engineering, Chongqing University, China

kaijieren@cqu.edu.cn, leizhang@cqu.edu.cn

Abstract

Visible-Infrared Person Re-identification (VI-ReID) is a challenging cross-modal pedestrian retrieval task, due to significant intra-class variations and cross-modal discrepancies among different cameras. Existing works mainly focus on embedding images of different modalities into a unified space to mine modality-shared features. They only seek distinctive information within these shared features, while ignoring the identity-aware useful information that is implicit in the modality-specific features. To address this issue, we propose a novel Implicit Discriminative Knowledge Learning (IDKL) network to uncover and leverage the implicit discriminative information contained within the modality-specific. First, we extract modality-specific and modality-shared features using a novel dual-stream network. Then, the modality-specific features undergo purification to reduce their modality style discrepancies while preserving identity-aware discriminative knowledge. Subsequently, this kind of implicit knowledge is distilled into the modality-shared feature to enhance its distinctiveness. Finally, an alignment loss is proposed to minimize modality discrepancy on enhanced modality-shared features. Extensive experiments on multiple public datasets demonstrate the superiority of IDKL network over the state-of-the-art methods. Code is available at <https://github.com/1KK077/IDKL>.

1. Introduction

Visible-Infrared Person Re-Identification (VI-ReID) aims to match pedestrian images across multiple non-overlapping camera views and different modalities. Advanced surveillance systems today are capable of automatically switching from visible to infrared mode at nightfall, ensuring an ample supply of trainable data. However, the unique modality of infrared images create significant domain discrepancies and a more complex environment. This makes previous single-modality methods, which are based

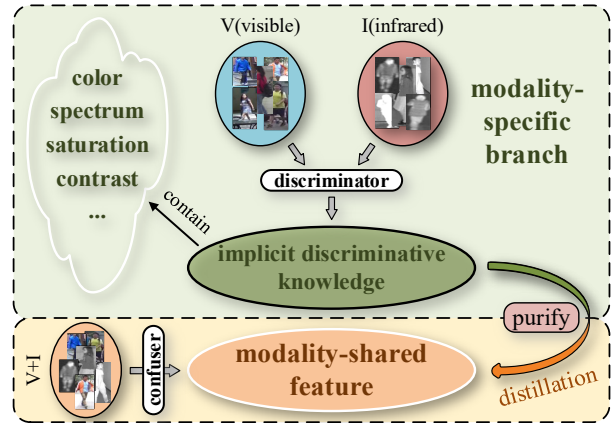


Figure 1. Previous methods focused on seeking discriminative information within modality-shared features, overlooking the fact that there are discriminative clues implicit in modality-specific features. It is worth considering utilization of the implicit discriminative information to enhance shared invariant feature.

solely on visible images, less efficient for VI-ReID tasks.

Recently, numerous advanced methods have emerged in the field of VI-ReID. In conclusion, these approaches can generally be categorized into two types: the first aims to learn modality-shared features directly from raw modal data, and the second seeks to incorporate additional modal information to refine the feature space or bridge the modal gap, thereby facilitating the search for modality-shared features. Raw modal data based method [2, 4, 7, 8, 17, 19, 33, 49] is to embed different modality images into the same space and align them on feature-level so that model learn modality invariant feature directly. Despite original images based methods has achieved desirable results, they still remain a huge gap between different modalities in feature space. In order to bridge the gap between visible and infrared modalities and construct a continuous space for better learning modality-shared features, various methods based on introducing extra information [14, 29, 30, 34, 38, 42, 45] have emerged constantly.

Although significant improvements have been made in

current VI-ReID methods, these models inevitably discard some discriminative information that relies on modality-specific features, which is not fully exploited and utilized previously. These discriminative cues that exist in modality-specific features can be referred to as implicit discriminative information, as shown by the green area in Fig. 1, such as color, grayscale spectrum, contrast, saturation, and so on. Therefore, relying solely on modality-shared cues can limit the upper boundary of the discrimination ability of the feature representation. Utilizing implicit modality-specific characteristics effectively is essential to enhance the distinctiveness of modality-invariant features. However, we cannot directly use the modality-specific knowledge due to the modality discrepancies it contains. Instead, we need to reduce these discrepancies while preserving the identity-aware discriminative information inherent in the implicit knowledge. Meanwhile, traditional VI-ReID methods involving distillation, alignment, and mutual learning typically rely on logits [35, 44, 47]. However, there is no involvement of the classifier during the testing phase, with matching performed only at the feature level. Therefore, conducting discriminative information distillation at the feature level is also essential.

To address the above limitations, in this paper, we propose an Implicit Discriminative Knowledge Learning (IDKL) framework that captures implicit invariant information from modality-specific features and distills it into modality-shared features to enhance their discriminative capability. We first extract modality-specific and modality-shared features using the modality discriminator and modality confuser, respectively. The modality discriminator effectively distinguishes between different modal features, endowing them with specific characteristics; whereas the modality confuser is unable to differentiate between modal features, thereby imparting shared characteristics to them. Since the modality-specific feature after previous stage contains substantial modality discrepancies, it is not suitable for direct distillation into the shared feature. We initially employ Instance Normalization to reduce domain discrepancies. However, it is crucial to acknowledge that IN inevitably results in the loss of some discriminative features. Therefore, we aim to reduce its modality style discrepancy while preserving identity-aware discriminative knowledge. Subsequently, we distill this implicit knowledge into the modality-shared feature at both the feature-level through feature graph structure, and the semantic-level through the logit vector to enhance its distinctiveness. Finally, an alignment loss is proposed to minimize modality discrepancy on enhanced modality-shared features.

The main contributions of this paper can be summarized as follows:

- We propose the Implicit Discriminative Knowledge Learning (IDKL) network to utilize the discriminative

knowledge implicit in the modality-specific features to enhance the upper bound of discriminative power for the modality-shared feature.

- To reduce the modality style discrepancy without losing discriminative information of modality-specific information, we propose an IN-guided Information Purifier (IP), which is supervised by the discrimination enhancing loss and discrepancy reducing loss.
- The novel TGSA loss is developed to distill the discriminative modality-specific information into modality-shared feature and mitigate inter-modality discrepancy of modality-shared feature sufficiently. The substantial experimental results demonstrate the superiority of our method.

2. Related Work

Visible Modality Person ReID. Person ReID has received increasing success in recent years, which aims to implement pedestrian retrieval between visible images. It has suffered huge challenges including various viewpoints, illuminations, postures and so on. To solve these problems, most methodologies [24, 25, 39, 48] are designed to obtain unified intra-class and discriminative inter-class representation by training CNN network. To further enhance the distinguishability of features, Sun *et al.* [27] proposed aligning part feature directly instead of using external cues. He *et al.* [9] caught the hot spot of transformer and first proposed the transformer variant applying on single-modality person ReID. Simultaneously, person ReID has developed some significant branches yet, such as Unsupervised Domain Adaptive Person ReID (UDA-ReID) and Domain Generalization Person ReID (DG-ReID) [41]. Although existing methods have made wide progress in visible modality person ReID, they suffer performance degradation when applied to visible-infrared person ReID due to the severe cross-modality discrepancy.

Visible-Infrared Person ReID (VI-ReID). VI-ReID is a cross-modality person retrieval problem, which aims at matching daytime visible and nighttime infrared images. It not only faces difficulties encountered in traditional single-modality person ReID task, but also the main challenge of huge modality discrepancy which caused by different camera spectra. To solve these issues, numerous approaches are proposed to search shared feature [1, 5, 18, 20, 32, 36, 39, 46]. Wu *et al.* [32] first formulated the VI-ReID issue and contributed a new cross-modality dataset SYSU-MM01, which is of great significance to the following research. Ye *et al.* [36] proposed a part-level feature interaction and graph structure attention to enhance the discrimination of invariant feature. Meanwhile, some work begin to introduce additional modal information to jointly search for invariant features [14, 21, 28, 30, 45]. Wang *et al.* [30] combined RGB three channels feature and IR single

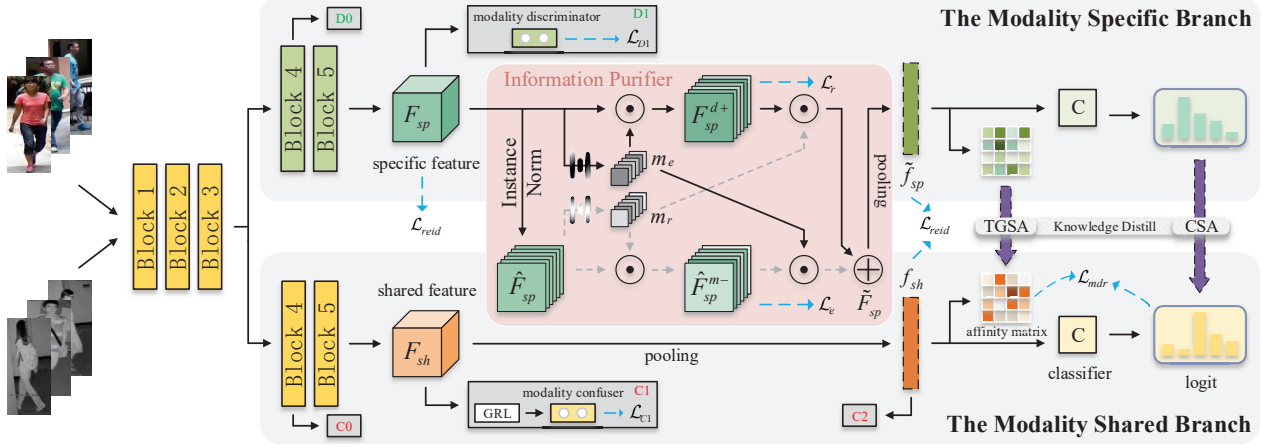


Figure 2. Framework of the proposed Implicit Discriminative Knowledge Learning (IDKL) model. The dual one-stream network built by resnet blocks first extracts the modality-specific F_{sp} and modality shared feature F_{sh} under the constraint of modality discriminator and modality confuser accordingly, while the common ReID loss is used to optimize network basely. Then, the modality-specific feature is fed into the information purifier to regulate the modality style discrepancy while preserving the implicit discriminative information and obtain the purified modality-specific feature \tilde{F}_{sp} . Subsequently, this implicit knowledge is distilled into the modality-shared feature through TGSA and CSA. Finally, the \mathcal{L}_{mdr} is further proposed to minimize modality discrepancy within the enhanced modality-shared feature.

channel feature into united four channels feature to reduce modal differences. Jiang *et al.* [14] employed a global prototype to generate the missing modality counterpart through transformer. However, these generation based compensation methods inevitably introduce much noise and most of present methods aim to align modal discrepancy and extract modality invariant feature. They ignored use of beneficial style information contained in specific features to increase distinctiveness.

Interactive Learning. In knowledge distillation, a teacher-student model is used to transfer the knowledge learned by a larger complex teacher model to a smaller simple student model. Different from the one-way transfer between a teacher and a student, deep mutual learning [44] is an ensemble of students which learns collaboratively and teaches each other throughout the training process. Some work applied this idea into VI-ReID for interactive learning in different modalities. Zheng *et al.* [47] enhanced invariant features learning by using interactive learning between two modality. Ye *et al.* [35] employed multi-classifier to reduce modality discrepancy on logits-level. Wu *et al.* [33] distilled RGB and IR knowledge mutually by four classifier to achieve inter shared representation. However, they only learn the knowledge within the semantic-level.

3. Methodology

In this section, we detail the proposed Implicit Discriminative Knowledge Learning (IDKL) framework as shown in Fig. 2. IDKL first distinguishes modality-specific features from modality-shared features through two network branches, which are constrained by modality discriminator

and modality confuser, respectively. Simultaneously, common ReID loss is used to endow feature with representation. Then, an Information Purifier (IP) is developed to reduce the impact of style variances while retaining identity-aware and discriminative knowledge in modality-specific features. Finally, we distill the implicit discriminative knowledge across two branches into the modality-shared feature through Triplet Graph Structure Alignment (TGSA) at the feature-level and Class Semantic Alignment (CSA) at the logit-level. Additionally, to reduce modality discrepancy of shared feature, we proposed the Modality Discrepancy Reduction (MDR) loss within the modality-shared branch. As the discriminative information increases and modality discrepancy decreases constantly, the enhanced modality-shared feature can be obtained.

Formally, we represent visible and infrared images in a dataset as $V = \{\mathbf{x}_i^V\}_{i=1}^{N_V}$ and $I = \{\mathbf{x}_i^I\}_{i=1}^{N_I}$, respectively. Typically, the number of images sampled in a mini-batch is equal across both modalities, i.e., $N_V = N_I = N = P \times K$, where N_V and N_I denote the number of images sampled from the visible and infrared modalities, respectively. Here, N represents the number of images from a single modality, $2N$ is the total number of images in a mini-batch, P is the number of distinct person classes, and K is the number of images from each class within a single modality. We can therefore represent the images and their corresponding labels in a mini-batch as $X = \{\mathbf{x}_i | \mathbf{x}_i \in V \cup I\}_{i=1}^{2N}$ and $Y = \{\mathbf{y}_i\}_{i=1}^{N_p=P}$, respectively. These images X are fed into two separate network branches to extract the modality-specific features F_{sp} which contains $F_{sp,V}$, $F_{sp,I}$ and the shared features F_{sh} which contains $F_{sh,V}$, $F_{sh,I}$ as fol-

lows:

$$\mathbf{F}_{sp} = E_{sp}(\mathbf{x} \mid \Theta, \Psi), \mathbf{F}_{sh} = E_{sh}(\mathbf{x} \mid \Theta, \Phi), \quad (1)$$

where E_{sp} and E_{sh} denote the specific and the shared feature extractor by employing ResNet-50, respectively. Among the structures of ResNet-50, the global average pooling replaced by Gem pooling[24, 39] which is a pooling operation between maximum pooling and average pooling. And Θ is the shallow layer parameters with the first three blocks of ResNet-50, Ψ and Φ is the deep layer parameters of different branches with the last two blocks of ResNet-50.

3.1. Modality Confuser and Discriminator

Modality Confuser. For each sample image x_i , there is a modality label $t_i \in \{0, 1\}$. To learn modality-irrelated shared information, similar to [6], our goal is to confuse different domains such that a domain classifier cannot distinguish the domain of origin for a sample. We employ an adversarial modality classifier based on the Gradient Reversed Layer (GRL) as the modality confuser. The constraint loss for the modality confuser is given by:

$$\mathcal{L}_{Cj} = -\frac{1}{2N} \sum_{i=1}^{2N} t_i \cdot \log p(C_j(GRL(\mathbf{F}_{sh}^i))), \quad (2)$$

where C_j represents the j -th modality confuser in the modality-shared branch, $p(\cdot)$ is the prediction probability obtained via the softmax function, and t_i is the modality label.

Modality Discriminator. To adequately learn modality-related specific information, we employ a modality classifier as the Modality Discriminator. This classifier, which does not use GRL, is applied on the specific branch to extract modality-specific features. The classification loss is formulated as follows:

$$\mathcal{L}_{Dj} = -\frac{1}{2N} \sum_{i=1}^{2N} t_i \cdot \log p(D_j(\mathbf{F}_{sp}^i)), \quad (3)$$

where D_j denotes the j -th modality discriminator in the modality-specific branch.

The combined loss from the modality confuser and discriminator is given by:

$$\mathcal{L}_C = \sum_{j=1}^K \mathcal{L}_{Cj}, \quad \mathcal{L}_D = \sum_{j=1}^K \mathcal{L}_{Dj}. \quad (4)$$

To efficiently extract both modality-specific and modality-shared features, we combine these modality classifier losses with the standard ReID loss \mathcal{L}_{reid} , which includes cross-entropy and hard triplet loss. These are applied to both the modality-specific and modality-shared branches as follows:

$$\mathcal{L}_{sp} = \mathcal{L}_{reid}(\mathbf{f}_{sp}) + \mathcal{L}_D, \quad \mathcal{L}_{sh} = \mathcal{L}_{reid}(\mathbf{f}_{sh}) + \mathcal{L}_C, \quad (5)$$

where $\mathbf{f} \in \mathbb{R}^{B \times C}$ is the pooling feature corresponding to $\mathbf{F} \in \mathbb{R}^{B \times C \times H \times W}$.

Thus, the base loss for our model is formulated as:

$$\mathcal{L}_b = \mathcal{L}_{sh} + \mathcal{L}_{sp}. \quad (6)$$

3.2. Information Purifier

The Information Purifier (IP) is designed to minimize the impact of style variances while retaining identity-aware and discriminative knowledge in modality-specific features. The IP integrates Instance Normalization (IN), which is known to reduce domain discrepancies [13, 23, 48]. However, it is important to recognize that IN inevitably leads to the loss of some discriminative features [11, 15], potentially hindering the high performance of ReID.

To overcome the aforementioned issues, we have designed a dual-mask network guided by Instance Normalization (IN) to alleviate modality style discrepancies while preserving implicit discriminative knowledge. Firstly, we apply IN on the modality-specific feature to obtain the normalized feature $\hat{\mathbf{F}}_{sp}$ by:

$$\hat{\mathbf{F}}_{sp} = \text{IN}(\mathbf{F}_{sp}) = \frac{\mathbf{F}_{sp} - \text{E}[\mathbf{F}_{sp}]}{\sqrt{\text{Var}[\mathbf{F}_{sp}] + \epsilon}}, \quad (7)$$

where the ϵ represents a safety factor to ensure the denominator is not zero. The mean $\text{E}[\cdot]$ and variance $\text{Var}[\cdot]$ are calculated along each channel.

Following the approach of SE-Net [10], we generate two channel-wise masks \mathbf{m}_e and \mathbf{m}_r by:

$$\mathbf{m}_e = \sigma(W_2 \delta(W_1 g(\mathbf{F}_{sp}))), \quad \mathbf{m}_r = \sigma(W_4 \delta(W_3 g(\hat{\mathbf{F}}_{sp}))), \quad (8)$$

where $g(\cdot)$ denotes the pooling operation, $W_1, W_3 \in \mathbb{R}^{\frac{c}{r} \times c}$ and $W_2, W_4 \in \mathbb{R}^{c \times \frac{c}{r}}$ are learnable parameters in the four fully-connected (FC) layers which are followed by the ReLU activation function $\delta(\cdot)$ and the sigmoid activation function $\sigma(\cdot)$. To balance the calculate consumption, the dimension reduction ratio r is set to 16.

The channel-wise masks \mathbf{m}_e and \mathbf{m}_r indicate enhancement of discriminative characteristics and reduction of discrepancies attention mask, respectively. So we can obtain the stronger distinctiveness \mathbf{F}_{sp}^{d+} and the smaller modality differences $\hat{\mathbf{F}}_{sp}^{m-}$ by:

$$\mathbf{F}_{sp}^{d+} = \mathbf{m}_e \odot \mathbf{F}_{sp}, \quad \hat{\mathbf{F}}_{sp}^{m-} = \mathbf{m}_r \odot \hat{\mathbf{F}}_{sp}. \quad (9)$$

Subsequently, the discrimination enhancing loss \mathcal{L}_e and the discrepancy reducing loss \mathcal{L}_r are calculated to supervise \mathbf{m}_e and \mathbf{m}_r respectively as:

$$\mathcal{L}_e = \text{Softplus} \left(h \left(C_{sp}(\mathbf{f}_{sp}^{d+}) \right) - h(C_{sp}(\mathbf{f}_{sp})) \right), \quad (10)$$

$$\mathcal{L}_r = \text{Softplus} \left(d \left(\hat{\mathbf{f}}_{sp,V}^{m-}, \hat{\mathbf{f}}_{sp,I}^{m-} \right) - d \left(\hat{\mathbf{f}}_{sp,V}, \hat{\mathbf{f}}_{sp,I} \right) \right). \quad (11)$$

Here, \mathcal{L}_e aims to imbue the generated \mathbf{F}_{sp}^{d+} with greater semantic distinctiveness compared to \mathbf{F}_{sp} , while \mathcal{L}_r seeks to ensure that $\widehat{\mathbf{F}}_{sp}^{m-}$ exhibit smaller modality differences than $\widehat{\mathbf{F}}_{sp}$. And $\text{Softplus}(\cdot) = \ln(1 + \exp(\cdot))$ is a function with monotonic increase, designed to alleviate optimization challenges by circumventing negative values in loss.

Finally, an alternating integration strategy is employed to extract the distinctive information from $\widehat{\mathbf{F}}_{sp}^{m-}$ by applying \mathbf{m}_e and the invariant information from \mathbf{F}_{sp}^{d+} by applying \mathbf{m}_r . Thus, The two sets of features extracted in this way both demonstrate smaller modality differences and stronger implicit discriminative information. By integrating them, we derive the purified modality-specific feature $\widetilde{\mathbf{F}}_{sp}$ as:

$$\widetilde{\mathbf{F}}_{sp} = \mathbf{m}_e \odot \widehat{\mathbf{F}}_{sp}^{m-} + \mathbf{m}_r \odot \mathbf{F}_{sp}^{d+}. \quad (12)$$

Intuitively, the pooling feature $\widetilde{\mathbf{f}}_{sp}$ of implicit feature $\widetilde{\mathbf{F}}_{sp}$ is also constraint with ReID loss. So the information purify loss \mathcal{L}_{ip} of this section is summarized as:

$$\mathcal{L}_{ip} = \mathcal{L}_e + \mathcal{L}_r + \mathcal{L}_{reid}(\widetilde{\mathbf{f}}_{sp}). \quad (13)$$

3.3. Implicit Knowledge Distillation

To ensure that the modality-shared feature comprehensively learns and integrates implicit information, we perform distillation from both the feature-level through TGSA and logit-level through CSA.

3.3.1 Triplet Graph Structure Alignment (TGSA)

To endow the shared feature with discriminative information and reduce modality discrepancy at the feature level, we develop a triplet feature graph structure alignment loss. This approach is motivated by the fact that the feature graph structure contains abundant information about the relationships and distribution between features, such as inter-class distinctiveness and intra-class diversity. These characteristics are utilized to unearth potential feature relationships and enhance the feature representation in [17, 36]. The graph structure affinity matrix which indicates the relationships between features is calculated by:

$$\alpha_{ij} = \frac{\exp(L([\mathbf{l}(\mathbf{f}_i) \parallel \mathbf{l}(\mathbf{f}_j)] \cdot \mathbf{w}))}{\sum_{k \in \mathcal{N}_i} \exp(L([\mathbf{l}(\mathbf{f}_i) \parallel \mathbf{l}(\mathbf{f}_k)] \cdot \mathbf{w}))}, \quad (14)$$

where the L denote LeakyReLU activation function, $[\cdot \parallel \cdot]$ denote concatenate operation and \mathcal{N}_i denotes the neighbor samples which are used to normalize for the i th sample. $\mathbf{l}(\cdot)$ is feature dimension transformation layer and \mathbf{w} is the full connection layer to calculate scores in a pair features. The affinity matrix is acquired making these scores through softmax function normalization.

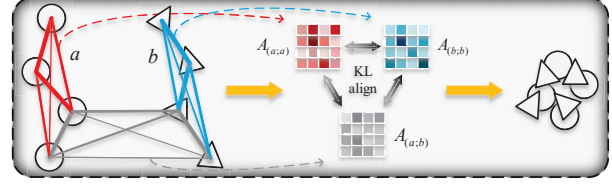


Figure 3. Illustration of the proposed TGSA loss: 'a' and 'b' denote two different types of features. 'A' represents the graph structure affinity matrix. After aligning the three affinity matrices, the discrepancy in the graph structure distribution between features 'a' and features 'b' will be eliminated.

Due to we utilize graph structure to align and distill knowledge, instead of augmenting the feature, and the Euclidean space distribution is more interesting for features, thus we replace the linear transformation with Euclidean distance to compute attention scores and redefine the graph structure expression for two groups of features as follows:

$$\mathbf{A}_{(a;b)} = \{\alpha_{ij}\}_{i,j \in N} = \frac{\exp(D(\mathbf{f}_a^i, \mathbf{f}_b^j))}{\sum_{k \in N} \exp(D(\mathbf{f}_a^i, \mathbf{f}_b^k))}, \quad (15)$$

where α_{ij} denotes the element of the affinity matrix, N corresponds to the entirety of samples within one modality, a and b represent two modalities, $D(\cdot)$ means Euclidean distance.

Specifically, the triplet graph structure alignment loss \mathcal{L}_{tgsa} is developed for cross modality ReID to align two different modality types, enabling them to conform to the same graph structure distribution and reduce modality discrepancy. This loss encompasses two self-modal affinity matrices and one cross-modal affinity matrix, with the latter ensuring the overall consistency of the graph structure's distribution as shown in Fig. 3. These three matrices are aligned pairwise through the utilization of the Kullback-Leibler (KL) divergence. Therefore, the alignment loss \mathcal{L}_{tgsa} of two distinct modality types is defined as:

$$\mathcal{L}_{tgsa}^{(a;b)} = \sum_{p=1}^P \sum_{k=1}^K \left(\text{KL}(\mathbf{A}_{(a;a)}^{pk}, \mathbf{A}_{(b;b)}^{pk}) + \text{KL}(\mathbf{A}_{(a;a)}^{pk}, \mathbf{A}_{(a;b)}^{pk}) + \text{KL}(\mathbf{A}_{(a;b)}^{pk}, \mathbf{A}_{(b;b)}^{pk}) \right). \quad (16)$$

Here, \mathbf{A}^{pk} represents the graph structure distribution of the k -th sample in the p -th class, where P is the number of person classes, and K denotes the number of images for each class within a single modality.

In order to convey the discriminative implicit modality-specific knowledge to shared feature on feature-level, the distillation loss across two branches on homogeneous features through TGSA can be formulated as:

$$\mathcal{L}_{tgsa} = \mathcal{L}_{tgsa}^{(sp,V;sh,V)} + \mathcal{L}_{tgsa}^{(sp,I;sh,I)}. \quad (17)$$

3.3.2 Class Sematic Alignment (CSA)

CSA is used to distill the semantic information of implicit modality-specific knowledge into the modality-shared branch for enhancing the feature representation of shared features. CSA operates on homogeneous features between two branches at logit-level. The logit matrix behind the classifier can be formulated as:

$$\mathbf{Z}_{sp} = C_{sp}(\mathbf{f}_{sp}), \mathbf{Z}_{sh} = C_{sh}(\mathbf{f}_{sh}), \quad (18)$$

where C_{sp} and C_{sh} is the modality-specific and modality-shared classifier separately. And the logit \mathbf{Z}_{sp} and $\mathbf{Z}_{sh} \in \mathbb{R}^{2N \times C}$ of specific and shared branch both contain visible modality and infrared modality, C is the total number of train dataset identities.

For learning the implicit discriminative modality-specific knowledge on semantic-level, the CSA loss is implemented on the same modality logit between the two branches, which is formulated as:

$$\mathcal{L}_{csa} = \sum_{i=1}^N (\text{KL}(\mathbf{Z}_{sh,V}^i, \mathbf{Z}_{sp,V}^i) + \text{KL}(\mathbf{Z}_{sh,I}^i, \mathbf{Z}_{sp,I}^i)). \quad (19)$$

3.4. Modality Discrepancy Reduction (MDR)

At this part, to guarantee the invariant representation of modality-shared feature, the TGSA and CSA are further used to reduce modality discrepancy within modality-shared branch as follow:

$$\mathcal{L}_{mdr} = \mathcal{L}_{tgsa}^{(sh,V;sh,I)} + \sum_{i=1}^N \text{KL}(\mathbf{Z}_{sh,V}^i, \mathbf{Z}_{sh,I}^i). \quad (20)$$

In this way, the visible feature and infrared feature in modality-shared branch can achieve mutual learning from feature-level and semantic-level. It makes two modalities feature aligning information each other, while alleviating modal gap and maintaining the invariant of modality-shared feature.

3.5. Optimization

Ultimately, by continuously distilling implicit discriminative knowledge from the modality-specific feature and consistently reducing modality discrepancies in the modality-shared feature, we can achieve a more discriminative and invariant modality-shared feature.

The total loss of the model IDKL is defined as:

$$\mathcal{L}_{total} = \mathcal{L}_b + \lambda_1 \mathcal{L}_{ip} + \lambda_2 \mathcal{L}_{tgsa} + \lambda_3 \mathcal{L}_{csa} + \mathcal{L}_{mdr}, \quad (21)$$

where λ_1 , λ_2 and λ_3 are hype-parameters to balance the contribution of individual loss term.

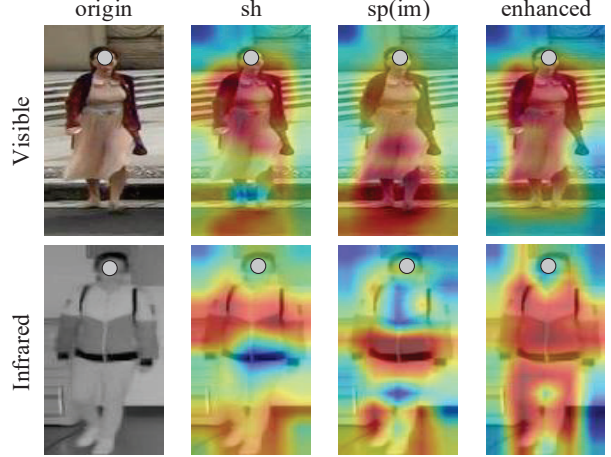


Figure 4. Observation the implicit discriminative information by Grad-CAM. And 'sh' and 'sp(im)' present the modality-shared feature and the modality-specific feature of trained IDKL w/o knowledge distillation, respectively; 'enhanced' denotes the modality-shared feature of IDKL w/ knowledge distillation.

4. Experiments

4.1. Datasets and Experimental Settings

Datasets. Three public VI-ReID datasets SYSU-MM01 [28], LLCM [43] and RegDB [22] are employed to evaluate our model. SYSU-MM01 is a popular large-scale dataset collected by four visible cameras and two near-infrared cameras, including indoor and outdoor environments. And the test protocols consist of all-search and indoor-search. LLCM dataset is a large-scale and low-light cross-modality dataset, which is divided into training and testing sets at a 2:1 ratio. RegDB is collected using dual-camera systems, where visible and infrared images are captured in pairs. Both LLCM and RegDB contain visible to infrared and infrared to visible two search modes.

Evaluation metrics. The standard rank- k matching accuracy and mean Average Precision (mAP) are adopted as the evaluation metrics. All the reported results are the average of 10 trials.

Implementation details. The proposed method and all experiments are implemented on a single NVIDIA GeForce 3090 GPU with PyTorch framework. The baseline model adopts the ResNet-50 pre-trained on ImageNet with the \mathcal{L}_b . The input images are resized to $3 \times 384 \times 128$. The train mini-batch size is set as 120, which contains 12 random identities and 10 images for every identity. Adam optimizer with an initial learning rate 3×10^{-5} is exploited, which decays at the 60th and 100th epoch with a decay factor of 0.1. The hype-parameters λ_1 , λ_2 and λ_3 are set to 0.1, 0.6 and 0.8. During the testing phase, only modality-shared feature is used to evaluate performance.

Table 1. Comparison of CMC (%) and mAP (%) performances with the state-of-the-art methods on **SYSU-MM01** dataset.

Methods	All-search							Indoor-search								
	Single-shot			Multi-shot				Single-shot			Multi-shot					
	r=1	r=10	r=20	map	r=1	r=10	r=20	map	r=1	r=10	r=20	map	r=1	r=10	r=20	map
Zero-Padding [32]	14.80	54.12	71.33	15.95	19.13	61.40	78.41	10.89	20.58	68.38	85.79	26.92	24.43	75.86	91.32	18.86
D-HSME [8]	20.68	62.74	77.95	23.12	-	-	-	-	-	-	-	-	-	-	-	-
AlignGAN [28]	42.40	85.00	93.70	40.70	51.50	89.40	95.70	33.90	45.90	87.60	94.40	54.30	57.10	92.70	97.40	45.30
DDAG [36]	54.75	90.39	95.81	53.02	-	-	-	-	61.02	94.06	98.41	67.98	-	-	-	-
NFS [2]	56.91	91.34	96.52	55.45	63.51	94.42	97.81	48.56	62.79	96.53	99.07	69.79	70.03	97.70	99.51	61.45
PIC [47]	57.51	89.35	95.03	55.14	-	-	-	-	60.40	-	-	67.70	-	-	-	-
MID [12]	60.27	92.90	-	59.40	-	-	-	-	64.86	96.12	-	70.12	-	-	-	-
cm-SSFT [21]	61.60	89.20	93.90	63.20	63.40	91.20	95.70	62.00	70.50	94.90	97.70	72.60	73.00	96.30	99.10	72.40
MCLNet [7]	65.40	93.33	97.14	61.98	-	-	-	-	72.56	96.98	99.20	76.58	-	-	-	-
FMCNet [42]	66.34	-	-	62.51	73.44	-	-	56.06	68.15	-	-	74.09	78.86	-	-	63.82
SMCL [31]	67.39	92.87	96.76	61.78	72.15	90.66	94.32	54.93	68.84	96.55	98.77	75.56	79.57	95.33	98.00	66.57
CAJ [37]	69.88	95.71	98.4	66.89	-	-	-	-	76.26	97.88	99.49	80.37	-	-	-	-
MPANet [33]	70.58	96.21	98.80	68.24	75.58	97.91	99.43	62.91	76.74	98.21	99.57	80.95	84.22	99.66	99.96	75.11
CMT [14]	71.88	96.45	98.87	68.57	80.23	97.91	99.53	63.13	76.9	97.68	99.64	79.91	84.87	99.41	99.97	74.11
DEEN [43]	74.7	97.6	99.2	71.8	-	-	-	-	80.3	99.0	99.8	83.3	-	-	-	-
SAAI [3]	75.90	-	-	77.03	82.8	-	-	82.39	83.20	-	-	88.01	90.73	-	-	91.30
MUN [40]	76.24	97.84	-	73.81	-	-	-	-	79.42	98.09	-	82.06	-	-	-	-
MSCLNet [45]	76.99	97.63	99.18	71.64	-	-	-	-	78.49	99.32	99.91	81.17	-	-	-	-
PartMix [16]	77.78	-	-	74.62	80.54	-	-	69.84	81.52	-	-	84.38	87.99	-	-	79.95
IDKL(Ours)	81.42	97.38	98.89	79.85	84.34	98.89	99.73	78.22	87.14	98.28	99.26	89.37	94.30	99.71	99.93	88.75

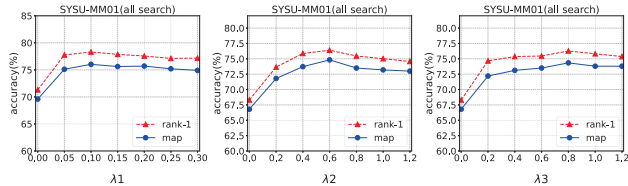


Figure 5. Ablation analysis of hyper-parameter λ_1 and λ_2 , λ_3 for \mathcal{L}_{ip} , \mathcal{L}_{tgsa} , and \mathcal{L}_{csa} respectively on SYSU-MM01 dataset.

4.2. Comparison with State-of-the-art Methods

We compare our IDKL model with the state-of-the-art VI-ReID methods published recent years on public VI-ReID datasets SYSU-MM01, RegDB and LLCM.

Comparison on SYSU-MM01 dataset. The comparison experimental results is shown in Tab. 1 which displays the proposed IDKL method outperforms existing cutting-edge methods. Specifically, the IDKL method achieves the accuracy of 81.42% rank-1 and 79.85% map with single-shot all search protocol, while the accuracy of 87.14% rank-1 and 89.37% map with single-shot indoor search protocol. The compared SOTAs include various base methods, *i.e.*, for the methods of learning the shared feature through network and loss function immediately, which contain D-HSME [8], NFS [2], CMT [14], DEEN[43] and MCLNet [7]. Based on graph structure augment method DDAG [36] and the mutual learning by logits skill (PIC [47] and MPANet [33]). Comparing with several other based modality-specific methods cm-SSFT[21], MUN[40] and MSCLNet[45], our results outperform them by a margin.

Comparison on RegDB dataset. We also evaluate IDKL on a small-scale dataset RegDB as shown in Tab. 2. There is strong performance IDKL showed and outperforms the existing solutions. Specifically, we achieve rank-1 ac-

curacy of 94.72% in visible to infrared mode, and rank-1 accuracy of 94.22% in infrared to visible mode.

Comparison on LLCM dataset. The IDKL model achieves significant improvements on the large and complex LLCM dataset as shown in Tab. 3, demonstrating excellent rank-1 accuracy of 72.2% and 70.7% on two modes, respectively. This indicates that the IDKL model exhibits strong robustness in complex and multimodal scenarios.

Table 2. Comparison of the CMC (%) and mAP (%) performances with state-of-the-art methods on **RegDB** dataset.

Methods	Visible to infrared		Infrared to visible	
	rank-1	map	rank-1	map
Zero-Padding [32]	17.8	18.9	16.7	17.9
AlignGAN [28]	57.9	53.6	56.3	53.4
DDAG [36]	69.34	63.46	68.06	61.80
cm-SSFT [21]	72.3	72.9	71.0	71.7
MCLNet [7]	80.31	73.07	75.93	69.49
PIC [47]	83.6	79.6	79.5	77.4
MPANet [33]	83.7	80.9	82.8	80.7
SMCL [31]	83.93	79.83	83.05	78.57
MSCLNet [45]	84.17	80.99	83.86	78.31
CAJ [37]	85.03	77.82	84.75	77.82
MID [12]	87.45	84.85	84.29	81.41
FMCNet [42]	89.12	84.43	88.38	83.86
SAAI [3]	91.07	91.45	92.09	92.01
DEEN [43]	91.1	85.1	89.5	83.4
CMT [14]	95.17	87.3	91.97	84.46
MUN [40]	95.19	87.15	91.86	85.01
IDKL(Ours)	94.72	90.19	94.22	90.43

4.3. Ablation Study

In this subsection, we conduct the ablation experiment to evaluate our proposed model exhaustively.

Table 3. Comparison of the CMC (%) and mAP (%) performances with state-of-the-art methods on **LLCM** dataset.

Methods	Visible to infrared		Infrared to visible	
	rank-1	map	rank-1	map
DDAG [36]	40.3	48.4	48.0	52.3
CAJ [37]	56.5	59.8	48.8	56.6
DEEN [43]	62.5	65.8	54.9	62.9
IDKL(Ours)	72.22	66.43	70.72	65.19

Table 4. Evaluation the impact of different components in terms of rank-1 (%) and mAP (%) on **SYSU-MM01** dataset.

\mathcal{L}_b	\mathcal{L}_{ip}	\mathcal{L}_{tgsa}	\mathcal{L}_{csa}	\mathcal{L}_{mdr}	SYSU-MM01	
					rank1	map
✓	×	×	×	×	67.60	66.47
✓	×	✓	×	×	68.38	67.30
✓	✓	✓	×	×	76.40	74.83
✓	✓	×	✓	×	76.28	74.34
✓	✓	×	×	✓	77.04	75.66
✓	✓	✓	✓	✓	81.42	79.85

Effectiveness of each component. We evaluate the effectiveness of each component on the SYSU-MM01 dataset under all search single-shot mode. Each component is added independently to reveal its the performance as Tab. 4. This indicates that each component is highly useful, with \mathcal{L}_{mdr} achieving significant performance improvements. This further suggests the effectiveness of TGSA and CSA in reducing modality discrepancies. Comparing the second row with the third row demonstrates the necessity of purifying implicit modality-specific information, and also proves the effectiveness of our Information Purifier module.

Hyper-parameters analysis of IP, TGSA and CSA. In this part, we present a line chart to examine the detail influence of IP, TGSA and CSA by gradually increasing the value of hyperparameters. As depicted in Fig. 5, the maximum contributions of IP, TGSA and CSA are reached at 0.1, 0.6 and 0.8, respectively. The upward trend of the curve demonstrates the effectiveness of each module.

4.4. Visualization Analysis

Attention maps Visualization. To further illustrate the effectiveness of IDKL, Grad-CAM [26] is utilized for a visual examination of different feature heatmaps. In Fig. 4, the areas of focus for implicit discriminative information typically differ from those of the shared feature, indicating that effectively and judiciously utilizing this information to strengthen the shared feature can be highly beneficial.

Feature Distribution Visualization. We utilize t-SNE [22] feature map visualization to observe the impact of the IDKL model and TGSA on the model. As shown in Fig. 6, each color represents a different identity, while the shapes of circles and triangles indicate the visible and infrared modality information, respectively. From Fig. 6(a),

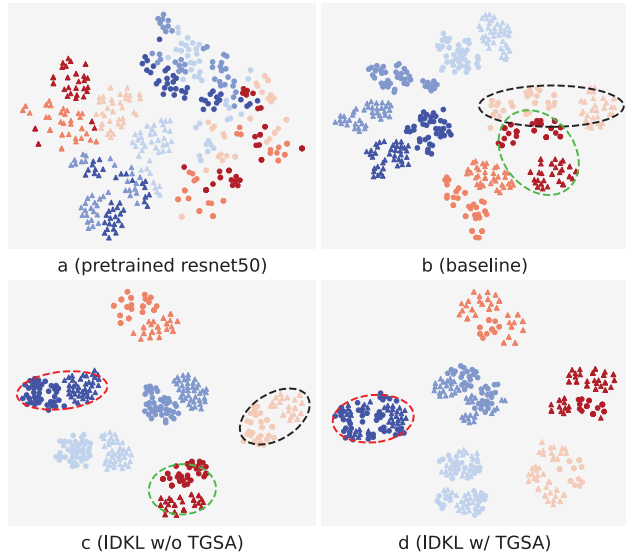


Figure 6. Visualization of learned features by t-SNE. Where "a" means the pre-training resnet50 on ImageNet; "b" represents the baseline; "c" is the IDKL model w/o TGSA; "d" is IDKL model w/ TGSA.

a significant discrepancy between the two modalities is evident. Fig. 6(b) shows a reduction in modality discrepancy and the model exhibiting some discriminative capabilities. Comparing Fig. 6(b) with Fig. 6(c), it is observable that the IDKL model has a smaller intra-class discrepancy and better inter-class discrimination. In Fig. 6(d), the dark blue class appears more scattered than in Fig. 6(c), and the graph structures of the two modalities are more similar and closely aligned, demonstrating the effectiveness of TGSA in reducing modality discrepancies.

5. Conclusion

This paper harnesses the implicit discriminative information within modality-specific features and introduces a robust model IDKL to exploit the potential discrimination of heterogeneous-related features and enhance the shared feature. The IDKL model comprises a dual one-stream network, a novel IN-guided information purifier, a triplet graph structure alignment solution, and refined distillation on logits. Collectively, these components demonstrate exceptional effectiveness and contribute to improved results.

Acknowledgments

This work was partially supported by National Key R&D Program of China (2021YFB3100800), National Natural Science Fund of China (62271090, 61771079), Chongqing Natural Science Fund (cstc2021jcyj-jqX0023) and National Youth Talent Project. This work is also supported by Huawei computational power of Chongqing Artificial Intelligence Innovation Center.

References

- [1] Cuiqun Chen, Mang Ye, Meibin Qi, Jingjing Wu, Jianguo Jiang, and Chia-Wen Lin. Structure-aware positional transformer for visible-infrared person re-identification. *IEEE Transactions on Image Processing*, 31:2352–2364, 2022. [2](#)
- [2] Yehansen Chen, Lin Wan, Zhihang Li, Qianyan Jing, and Zongyuan Sun. Neural feature search for rgb-infrared person re-identification. In *2021 IEEE/CVF Conference on Computer Vision and Pattern Recognition (CVPR)*, pages 587–597, 2021. [1](#), [7](#)
- [3] Xingye Fang, Yang Yang, and Ying Fu. Visible-infrared person re-identification via semantic alignment and affinity inference. In *Proceedings of the IEEE/CVF International Conference on Computer Vision*, pages 11270–11279, 2023. [7](#)
- [4] Chaoyou Fu, Yibo Hu, Xiang Wu, Hailin Shi, Tao Mei, and Ran He. Cm-nas: Cross-modality neural architecture search for visible-infrared person re-identification. In *2021 IEEE/CVF International Conference on Computer Vision (ICCV)*, pages 11803–11812, 2021. [1](#)
- [5] Xiaowei Fu, Fuxiang Huang, Yuhang Zhou, Huimin Ma, Xin Xu, and Lei Zhang. Cross-modal cross-domain dual alignment network for rgb-infrared person re-identification. *IEEE Transactions on Circuits and Systems for Video Technology*, 32(10):6874–6887, 2022. [2](#)
- [6] Yaroslav Ganin and Victor Lempitsky. Unsupervised domain adaptation by backpropagation. In *International conference on machine learning*, pages 1180–1189. PMLR, 2015. [4](#)
- [7] Xin Hao, Sanyuan Zhao, Mang Ye, and Jianbing Shen. Cross-modality person re-identification via modality confusion and center aggregation. In *2021 IEEE/CVF International Conference on Computer Vision (ICCV)*, pages 16383–16392, 2021. [1](#), [7](#)
- [8] Yi Hao, Nannan Wang, Jie Li, and Xinbo Gao. Hsme: Hypersphere manifold embedding for visible thermal person re-identification. In *Proceedings of the AAAI conference on artificial intelligence*, pages 8385–8392, 2019. [1](#), [7](#)
- [9] Shuting He, Hao Luo, Pichao Wang, Fan Wang, Hao Li, and Wei Jiang. Transreid: Transformer-based object re-identification. In *2021 IEEE/CVF International Conference on Computer Vision (ICCV)*, pages 14993–15002, 2021. [2](#)
- [10] Jie Hu, Li Shen, and Gang Sun. Squeeze-and-excitation networks. In *Proceedings of the IEEE conference on computer vision and pattern recognition*, pages 7132–7141, 2018. [4](#)
- [11] Xun Huang and Serge Belongie. Arbitrary style transfer in real-time with adaptive instance normalization. In *Proceedings of the IEEE international conference on computer vision*, pages 1501–1510, 2017. [4](#)
- [12] Zhipeng Huang, Jiawei Liu, Liang Li, Kecheng Zheng, and Zheng-Jun Zha. Modality-adaptive mixup and invariant decomposition for rgb-infrared person re-identification. In *Proceedings of the AAAI Conference on Artificial Intelligence*, pages 1034–1042, 2022. [7](#)
- [13] Jieru Jia, Qiuqi Ruan, and Timothy M Hospedales. Frustratingly easy person re-identification: Generalizing person re-id in practice. *arXiv preprint arXiv:1905.03422*, 2019. [4](#)
- [14] Kongzhu Jiang, Tianzhu Zhang, Xiang Liu, Bingqiao Qian, Yongdong Zhang, and Feng Wu. Cross-modality transformer for visible-infrared person re-identification. In *Computer Vision—ECCV 2022: 17th European Conference, Tel Aviv, Israel, October 23–27, 2022, Proceedings, Part XIV*, pages 480–496. Springer, 2022. [1](#), [2](#), [3](#), [7](#)
- [15] Xin Jin, Cuiling Lan, Wenjun Zeng, Zhibo Chen, and Li Zhang. Style normalization and restitution for generalizable person re-identification. In *proceedings of the IEEE/CVF conference on computer vision and pattern recognition*, pages 3143–3152, 2020. [4](#)
- [16] Minsu Kim, Seungryong Kim, Jungin Park, Seongheon Park, and Kwanghoon Sohn. Partmix: Regularization strategy to learn part discovery for visible-infrared person re-identification. In *Proceedings of the IEEE/CVF Conference on Computer Vision and Pattern Recognition*, pages 18621–18632, 2023. [7](#)
- [17] Xulin Li, Yan Lu, Bin Liu, Yating Liu, Guojun Yin, Qi Chu, Jinyang Huang, Feng Zhu, Rui Zhao, and Nenghai Yu. Counterfactual intervention feature transfer for visible-infrared person re-identification. In *Computer Vision—ECCV 2022: 17th European Conference, Tel Aviv, Israel, October 23–27, 2022, Proceedings, Part XXVI*, pages 381–398. Springer, 2022. [1](#), [5](#)
- [18] Wenqi Liang, Guangcong Wang, Jianhuang Lai, and Xiaohua Xie. Homogeneous-to-heterogeneous: Unsupervised learning for rgb-infrared person re-identification. *IEEE Transactions on Image Processing*, 30:6392–6407, 2021. [2](#)
- [19] Haijun Liu, Xiaoheng Tan, and Xichuan Zhou. Parameter sharing exploration and hetero-center triplet loss for visible-thermal person re-identification. *IEEE Transactions on Multimedia*, 23:4414–4425, 2021. [1](#)
- [20] Jialun Liu, Yifan Sun, Feng Zhu, Hongbin Pei, Yi Yang, and Wenhui Li. Learning memory-augmented unidirectional metrics for cross-modality person re-identification. In *2022 IEEE/CVF Conference on Computer Vision and Pattern Recognition (CVPR)*, pages 19344–19353, 2022. [2](#)
- [21] Yan Lu, Yue Wu, Bin Liu, Tianzhu Zhang, Baopu Li, Qi Chu, and Nenghai Yu. Cross-modality person re-identification with shared-specific feature transfer. In *2020 IEEE/CVF Conference on Computer Vision and Pattern Recognition (CVPR)*, pages 13376–13386, 2020. [2](#), [7](#)
- [22] Dat Tien Nguyen, Hyung Gil Hong, Ki Wan Kim, and Kang Ryoung Park. Person recognition system based on a combination of body images from visible light and thermal cameras. *Sensors*, 17(3):605, 2017. [6](#), [8](#)
- [23] Xingang Pan, Ping Luo, Jianping Shi, and Xiaoou Tang. Two at once: Enhancing learning and generalization capacities via ibn-net. In *Proceedings of the European Conference on Computer Vision (ECCV)*, pages 464–479, 2018. [4](#)
- [24] Filip Radenović, Giorgos Toliás, and Ondřej Chum. Fine-tuning cnn image retrieval with no human annotation. *IEEE Transactions on Pattern Analysis and Machine Intelligence*, 41(7):1655–1668, 2019. [2](#), [4](#)
- [25] Min Ren, Lingxiao He, Xingyu Liao, Wu Liu, Yunlong Wang, and Tieniu Tan. Learning instance-level spatial-temporal patterns for person re-identification. In *2021 IEEE/CVF International Conference on Computer Vision (ICCV)*, pages 14910–14919, 2021. [2](#)

- [26] Ramprasaath R Selvaraju, Michael Cogswell, Abhishek Das, Ramakrishna Vedantam, Devi Parikh, and Dhruv Batra. Grad-cam: Visual explanations from deep networks via gradient-based localization. In *Proceedings of the IEEE international conference on computer vision*, pages 618–626, 2017. 8
- [27] Yifan Sun, Liang Zheng, Yi Yang, Qi Tian, and Shengjin Wang. Beyond part models: Person retrieval with refined part pooling (and a strong convolutional baseline). In *Proceedings of the European conference on computer vision (ECCV)*, pages 480–496, 2018. 2
- [28] Guan'an Wang, Tianzhu Zhang, Jian Cheng, Si Liu, Yang Yang, and Zengguang Hou. Rgb-infrared cross-modality person re-identification via joint pixel and feature alignment. In *2019 IEEE/CVF International Conference on Computer Vision (ICCV)*, pages 3622–3631, 2019. 2, 6, 7
- [29] Guan-An Wang, Tianzhu Zhang, Yang Yang, Jian Cheng, Jianlong Chang, Xu Liang, and Zeng-Guang Hou. Cross-modality paired-images generation for rgb-infrared person re-identification. In *Proceedings of the AAAI conference on artificial intelligence*, pages 12144–12151, 2020. 1
- [30] Zhixiang Wang, Zheng Wang, Yinqiang Zheng, Yung-Yu Chuang, and Shin'ich Satoh. Learning to reduce dual-level discrepancy for infrared-visible person re-identification. In *2019 IEEE/CVF Conference on Computer Vision and Pattern Recognition (CVPR)*, pages 618–626, 2019. 1, 2
- [31] Ziyu Wei, Xi Yang, Nannan Wang, and Xinbo Gao. Syncretic modality collaborative learning for visible infrared person re-identification. In *2021 IEEE/CVF International Conference on Computer Vision (ICCV)*, pages 225–234, 2021. 7
- [32] Ancong Wu, Wei-Shi Zheng, Hong-Xing Yu, Shaogang Gong, and Jianhuang Lai. Rgb-infrared cross-modality person re-identification. In *2017 IEEE International Conference on Computer Vision (ICCV)*, pages 5390–5399, 2017. 2, 7
- [33] Qiong Wu, Pingyang Dai, Jie Chen, Chia-Wen Lin, Yongjian Wu, Feiyue Huang, Bineng Zhong, and Rongrong Ji. Discover cross-modality nuances for visible-infrared person re-identification. In *2021 IEEE/CVF Conference on Computer Vision and Pattern Recognition (CVPR)*, pages 4328–4337, 2021. 1, 3, 7
- [34] Yang Yang, Tianzhu Zhang, Jian Cheng, Zengguang Hou, Prayag Tiwari, Hari Mohan Pandey, et al. Cross-modality paired-images generation and augmentation for rgb-infrared person re-identification. *Neural Networks*, 128:294–304, 2020. 1
- [35] Mang Ye, Xiangyuan Lan, Qingming Leng, and Jianbing Shen. Cross-modality person re-identification via modality-aware collaborative ensemble learning. *IEEE Transactions on Image Processing*, 29:9387–9399, 2020. 2, 3
- [36] Mang Ye, Jianbing Shen, David J. Crandall, Ling Shao, and Jiebo Luo. Dynamic dual-attentive aggregation learning for visible-infrared person re-identification. In *Computer Vision–ECCV 2020: 16th European Conference, Glasgow, UK, August 23–28, 2020, Proceedings, Part XVII 16*, pages 229–247. Springer, 2020. 2, 5, 7, 8
- [37] Mang Ye, Weijian Ruan, Bo Du, and Mike Zheng Shou. Channel augmented joint learning for visible-infrared recognition. In *2021 IEEE/CVF International Conference on Computer Vision (ICCV)*, pages 13547–13556, 2021. 7, 8
- [38] Mang Ye, Jianbing Shen, and Ling Shao. Visible-infrared person re-identification via homogeneous augmented tri-modal learning. *IEEE Transactions on Information Forensics and Security*, 16:728–739, 2021. 1
- [39] Mang Ye, Jianbing Shen, Gaojie Lin, Tao Xiang, Ling Shao, and Steven C. H. Hoi. Deep learning for person re-identification: A survey and outlook. *IEEE Transactions on Pattern Analysis and Machine Intelligence*, 44(6):2872–2893, 2022. 2, 4
- [40] Hao Yu, Xu Cheng, Wei Peng, Weihao Liu, and Guoying Zhao. Modality unifying network for visible-infrared person re-identification. In *Proceedings of the IEEE/CVF International Conference on Computer Vision*, pages 11185–11195, 2023. 7
- [41] Lei Zhang, Zhipu Liu, Wensheng Zhang, and David Zhang. Style uncertainty based self-paced meta learning for generalizable person re-identification. *IEEE Transactions on Image Processing*, 32:2107–2119, 2023. 2
- [42] Qiang Zhang, Changzhou Lai, Jianan Liu, Nianchang Huang, and Jungong Han. Fmcnet: Feature-level modality compensation for visible-infrared person re-identification. In *2022 IEEE/CVF Conference on Computer Vision and Pattern Recognition (CVPR)*, pages 7339–7348, 2022. 1, 7
- [43] Yukang Zhang and Hanzi Wang. Diverse embedding expansion network and low-light cross-modality benchmark for visible-infrared person re-identification. In *Proceedings of the IEEE/CVF Conference on Computer Vision and Pattern Recognition*, pages 2153–2162, 2023. 6, 7, 8
- [44] Ying Zhang, Tao Xiang, Timothy M Hospedales, and Huchuan Lu. Deep mutual learning. In *Proceedings of the IEEE conference on computer vision and pattern recognition*, pages 4320–4328, 2018. 2, 3
- [45] Yiyuan Zhang, Sanyuan Zhao, Yuhao Kang, and Jianbing Shen. Modality synergy complement learning with cascaded aggregation for visible-infrared person re-identification. In *Computer Vision–ECCV 2022: 17th European Conference, Tel Aviv, Israel, October 23–27, 2022, Proceedings, Part XIV*, pages 462–479. Springer, 2022. 1, 2, 7
- [46] Jiaqi Zhao, Hanzheng Wang, Yong Zhou, Rui Yao, Silin Chen, and Abdulmotaleb El Saddik. Spatial-channel enhanced transformer for visible-infrared person re-identification. *IEEE Transactions on Multimedia*, pages 1–1, 2022. 2
- [47] Xiangtao Zheng, Xiumei Chen, and Xiaoqiang Lu. Visible-infrared person re-identification via partially interactive collaboration. *IEEE Transactions on Image Processing*, 31: 6951–6963, 2022. 2, 3, 7
- [48] Kaiyang Zhou, Yongxin Yang, Andrea Cavallaro, and Tao Xiang. Omni-scale feature learning for person re-identification. In *Proceedings of the IEEE/CVF international conference on computer vision*, pages 3702–3712, 2019. 2, 4
- [49] Yuanxin Zhu, Zhao Yang, Li Wang, Sai Zhao, Xiao Hu, and Dapeng Tao. Hetero-center loss for cross-modality person re-identification. *Neurocomputing*, 386:97–109, 2020. 1